High-Order Accurate Methods for High-Speed Flow

Georg May* and Antony Jameson†

This work focuses on high-order numerical schemes for conservation laws with emphasis on problems that admit discontinuous solutions. We will investigate several enabling techniques with the aim to construct robust methods for unstructured meshes capable of reliably producing globally high-order accurate results even in the presence of discontinuities. We use spectral and pseudo-spectral schemes in connection with such techniques as Gibbs-complementary reconstruction to recover high-order accuracy near discontinuities.

I. Introduction

Computational aerodynamics has been dominated by schemes which are higher than first-order accurate only in smooth regions, where they are typically restricted to second, or perhaps third order accuracy. The presence of discontinuities in transonic aerodynamics has greatly hampered the success of high-order accurate methods. In the vicinity of discontinuities the typical scheme uses restrictive limiters to damp out high-frequency oscillatory modes. While low-order schemes have been very successful due to their robustness and relative efficiency, many fields of research, such as aeroacoustics, large-eddy simulation (LES), and unsteady nonperiodic flow require highly accurate numerical methods. For many applications a high-order accurate scheme for solutions with discontinuities that retains its nominal accuracy everywhere would be quite welcome.

In this paper we will explore one possible route to such a scheme. We will start from a most promising new numerical scheme for unstructured meshes, namely the Spectral Difference method,[1] which combines elements from finite-volume and finite-difference techniques, and is particularly attractive because of its simple formulation and implementation.

It is well known that high-order accurate numerical schemes will produce oscillatory solutions for hyperbolic equations with discontinuities, if these are not prevented by using nonlinear limiters. The unlimited solution, if stabilized by high-order diffusion, exhibits oscillations of the order of what one would expect from Gibbs' phenomenon, if the analytical solution were to be expanded in smooth basis functions. In the absence of instabilities and if it is not destroyed by using limiting functions, it can be conjectured that information up to the nominal degree of accuracy is still present, in the sense established by the Gibbs-complementary reconstruction, which has been recently developed in a different context as a means of recovering high-order accurate smooth representations given spectral data for discontinuous functions. We investigate the extension of such methods to high-order approximations of partial differential equations. We confirm in this paper by strict measurements for nonlinear hyperbolic equations that indeed the full nominal order of accuracy can be recovered from the unlimited oscillatory solution. For the Euler equations, smooth solutions with perfect discontinuities and small absolute error are shown.

We discuss the Spectral Difference Method in section II. In section III we discuss the Gibbs complementary reconstruction, and point out how the rigorous theory developed for the method relates to the context in which it is used here. We show numerical results in section IV.

*PhD Candidate, Department of Aeronautics and Astronautics, Stanford University, AIAA Member.

†Thomas V. Jones Professor of Engineering, Department of Aeronautics and Astronautics, Stanford University, AIAA Member.

II. The Spectral Difference Method

The spectral difference method has quite recently been proposed by Liu et al.[1] and further developed by Wang et al.[2] We will restrict ourselves in this paper to the solution of equations of the form

$$\frac{\partial u}{\partial t} + \nabla \cdot F = 0 \tag{1}$$

on simplices, such as triangles in two dimensions. Suppose we are given a mesh of such elements. The Spectral Difference method uses a pseudo-spectral collocation-based reconstruction for both the dependent variables $u(x, y)$ and the flux function $F(u)$ inside each element. The reconstruction for the dependent variables can be written

$$u(x, y) = \sum_{j=1}^{N_u} L_j(x, y) u_j \tag{2}$$

Where L is the cardinal basis function for the given representation, and $u_j = u(x_j, y_j)$, where the $(x_j, y_j)^T$ are collocation points. Similarly one can write for the flux function

$$F(x, y) = \sum_{k=1}^{N_f} M_k(x, y) F_k \ , \tag{3}$$

where the M_k are the basis functions, and $F_k = F(u(x_k, y_k))$, where the $(x_k, y_k)^T$ are collocation points for the fluxes. The number of collocation points, N_u and N_f, are determined by the selected accuracy. In two dimensions, for accuracy n, one needs

$$N = \frac{n(n+1)}{2} \tag{4}$$

collocation points for the reconstruction of the solution. If the solution is reconstructed to order n, the flux nodes are interpolated to order $m = n+1$, because of the differentiation operation in equation 1. Figure 2 on page 4 shows examples of one- and two-dimensional stencils.

Given the dependent variables at the collocation points u_j, the solution is reconstructed in each cell and equation 2 is evaluated at flux collocation points k, i.e. with $L(x_k, y_k)$. Fluxes are then evaluated using the reconstructed values of u_k. The derivatives of these fluxes can be obtained by differentiating the basis function. Thus $\nabla \cdot F$ is obtained and evaluated at the solution collocation points using $\nabla M_k(x_j, y_j) \cdot F_k$ in equation 3, and the solution can be updated via equation 1 and a time integration scheme, such as a Runge-Kutta scheme. The method is closely related to staggered grid multidomain methods, proposed by Kopriva.[3] Here, in a sense, each simplex is a subdomain, and instead of tensor product forms of one-dimensional basis functions, we use two-dimensional collocation methods.

The key ingredient of the method is the flux evaluation of nodes located on the element boundaries, where the flux function will be multi-valued. For flux points located on edges it is necessary for discrete conservation that the normal flux component be the same for adjacent cells. This suggests the use numerical flux formulas used in standard finite-volume formulations, $F_n = h(u^l, u^r, \nu)$, where F_n is the normal flux and u^l and u^r are the reconstructed solution variables to the left and right of the edge, and ν is the edge normal. A schematic illustration is shown in figure 1(a) on the following page. For flux nodes on corners the optimal treatment is still an open problem. One may compute the corner fluxes from normal fluxes on the two incident edges of the triangles by imposing

$$\begin{aligned} F \cdot n_1 &= F_{n_1} \\ F \cdot n_2 &= F_{n_2} \ , \end{aligned} \tag{5}$$

which makes the flux unique and allows for conservation. The linear system, equation 5, can be solved analytically to give modified Riemann fluxes on corners that can be split into two parts, which are associated

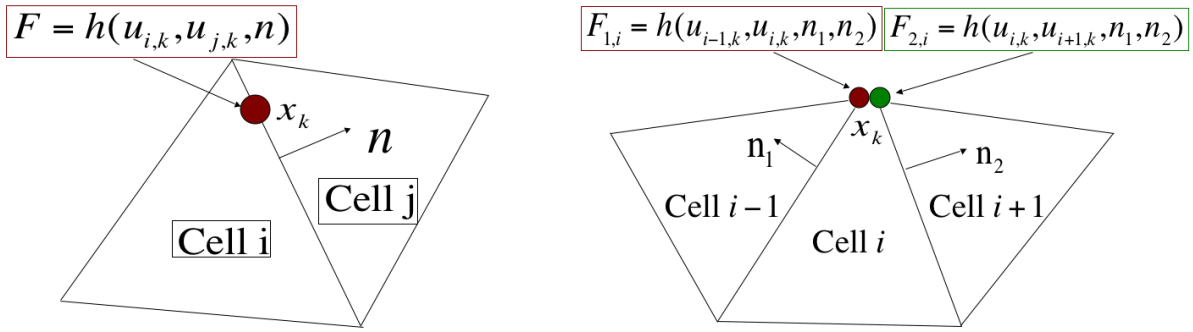

(a) Flux computation for points on edges

(b) Flux computation for points on corners

Figure 1. Illustration of flux computation for nodes on element boundaries.

with the two incident edges, that are used to computed the flux F. This is shown in figure 1(b). To show discrete conservation for the simplex in d dimensions, T_d, we must show that

$$\mathcal{I} = \frac{d}{dt}\int_{T_d} u\, dV + \int_{\partial T_d} \mathbf{F}\cdot\mathbf{n}\, dA = 0 \tag{6}$$

is recovered in the discrete approximation based on the collocation nodes. This imposes some restrictions as to the choice of collocation nodes. We show in the following that these restrictions can be recast in very simple form. Suppose u can be represented by a d-dimensional polynomial of degree at most n, and F is represented by a d-dimensional polynomial of degree at most $n+1$. We then have

$$\mathcal{I} = \frac{d}{dt}\int_{T_d} u\, dV = -\int_{T_d}\sum_{k=1}^{N_f}\nabla M_k\cdot\mathbf{F}_k\, dV = -V\sum_{j=1}^{N_u} w_j \sum_{k=1}^{N_f}\nabla M_k(\mathbf{x}_j)\cdot\mathbf{F}_k \tag{7}$$

Note that all the equalities are exact by construction, provided the collocation points for u support a quadrature with weights w_j, which is exact for polynomials of degree n.

Denote the elements of the differentiation matrices $\nabla M_k(\mathbf{x}_j) = \mathbf{m}_{kj}$, where each $\mathbf{m}_{kj}$ is a vector with d components. We have

$$\mathcal{I} = -V\sum_{k=1}^{N_f}\sum_{j=1}^{N_u} w_j\mathbf{m}_{kj}\cdot\mathbf{F}_k = -\sum_{k=1}^{N_f}\widetilde{\mathbf{w}}_k\cdot\mathbf{F}_k \tag{8}$$

We thus arrive at a modified quadrature using the flux points. The integral, however, must not depend on interior flux points. Indeed, we can write using the definition of the new weights $\widetilde{w}_k$:

$$\widetilde{\mathbf{w}}_k = V\sum_{j=1}^{N_u} w_j\mathbf{m}_{kj} = \int_{T_d}\nabla M_k(\mathbf{x})\, dV = \int_{\partial T_d} M_k\nu\, dA\ , \tag{9}$$

where ν is the outward pointing face normal on ∂T_d. The second equality is exact, because ∇M is a polynomial of degree n. Suppose the collocation points of F restricted to the boundaries of the simplex

support a $d-1$-dimensional quadrature of degree $n+1$ for each boundary $l = 1 \dots d$, with weights w_m^l, $m = 1 \dots N_e$, where N_e is the number of points on the boundaries. We then have the following exact relationship:

$$\widetilde{\mathbf{w}}_k = \int_{\partial T_d} M_k \nu \, dA = \sum_{l=1}^{d} \mathbf{S}^l \sum_{m=1}^{N_e} w_m^l M_k(\mathbf{x}_m) \ , \tag{10}$$

where S^l is the area of face l. But since M_k is an interpolation polynomial with the property $M_k(\mathbf{x}_m) = \delta_{km}$, this will simply pick out the weight w_k^l corresponding to the flux node k. In particular it is clear that the weight $\widetilde{w}_k$ for interior nodes vanish, since $k \neq m$ for all such nodes. We finally arrive at

$$\mathcal{I} = -\sum_{k=1}^{N_f} \widetilde{\mathbf{w}}_k \cdot \mathbf{F}_k = -\sum_{l=1}^{d} \sum_{m=1}^{N^e} \mathbf{w}_m^l \mathbf{F}_{k(l,m)} \cdot \mathbf{S}^l = -\int_{\partial T_n} \mathbf{F} \cdot d\mathbf{S} \tag{11}$$

In summary, then, we are free to choose any combination of collocation nodes, provided that the nodes for u support a quadrature of the order of the interpolation n, and the restriction of the flux nodes to the boundaries supports a $d-1$-dimensional quadrature of order $n+1$. For the solution nodes one can choose Gauss quadrature points. Hesthaven proposed nodes based on the solution of an electrostatics problem for simplices,[4] which support both a volume and a surface integration to the required degree of accuracy. These nodes have been used in this work for flux collocation. Figures 2(a) and 2(b) show examples of nodes which use a combination of these flux nodes with Gauss nodes for the solution. Since a volume integration is supported, we have also used staggered grids with nodes from[4] for both solution and flux functions. Such a stencil is shown in figure 2(c). For computations in one dimension Gauss and Gauss-Lobatto nodes can be

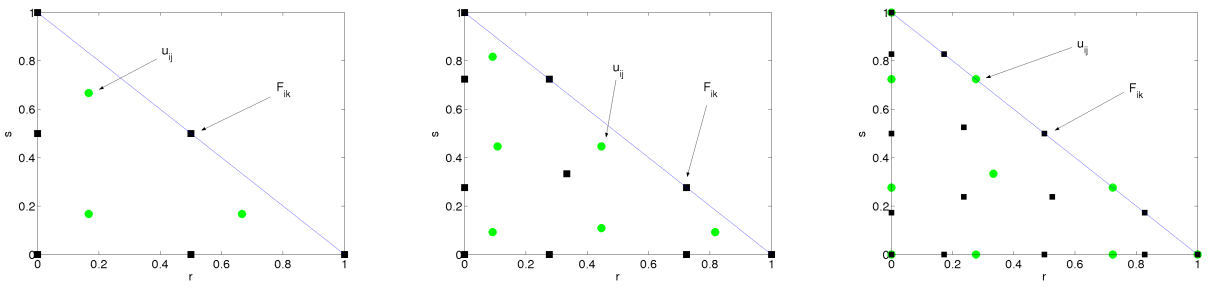

(a) Linear Triangle: (b) Quadratic Triangle (c) Cubic Triangle

Figure 2. Schematic depiction of collocation nodes for triangles.

used. No attempts have been made to optimize the choice with respect to running time. Some stencils share points between flux and solution nodes, which reduces the cost of the reconstruction. One can also choose a completely collocated set of nodes, which eliminates the reconstruction in equation 2 completely, at the cost of more expensive flux scattering procedure, due to the increased number of solution nodes.

The high-order reconstruction usually allows us to use simple flux functions on element boundaries such as a simple average with scalar dissipation. For example one can write for the normal flux component

$$F_n(u^l, u^r) = \frac{1}{2} \left\{ \left(f(u^l) + f(u^r) \right) \cdot \underline{n} - \alpha_n \left(u^r - u^l \right) \right\} \ , \tag{12}$$

where α is proportional to the spectral radius of the local flux Jacobian, $\alpha \propto u_n + c_n$, where u_n is the velocity normal to the edge, and c_n is the local speed of sound. We have also used the CUSP construction of artificial diffusion[5] instead of the simple dissipation of equation 12, in particular for the Euler equations. Tangential

flux components can either be evaluated in each cell and left unchanged or averaged across cell interfaces using an arithmetic average. For points in the interior of an element the flux function can be evaluated directly with the local state.

Normally limiter functions are used to promote monotonicity of numerical schemes for nonlinear conservation laws, which can be used to prove stability and convergence. This has been done for high-order methods, such as the Discontinuous Galerkin method.[6] As we discuss below we have explored the possibility of recovering solutions accurate in maximum norm without the use of such limiting functions. This requires stabilization of the numerical scheme in some appropriate fashion, certainly in the case of discontinuities. For smooth solutions, and generally for moderate orders of accuracy the high-order dissipation from the discontinuous states at the element boundaries is usually enough to render the scheme stable. More sophisticated approaches such as spectral viscosity methods[7] which operate explicitly on the high-frequency part of the spectrum could be used, and may find use in the future. For some one-dimensional results with discontinuities we have also used global filtering operations, such as adaptive exponential filters,[8] which attenuate the high-frequency Fourier spectrum, to stabilize the method.

III. Gibbs-Complementary Reconstruction for spectral/pseudo-spectral data

A. Basic Theory

For convenience we will present the theory for the Gibbs-complementary reconstruction for one-dimensional functions. Tensor products of the relevant basis functions can be used for the multidimensional extension. Assume that $N+1$ spectral coefficients b_k , $k = 0,\ldots,N$ of a *piecewise-smooth* function $f(x)$, defined on an interval, $[a, b]$ are given, such that

$$f_N(x) = \sum_{n=0}^{N} b_k \phi_k(x) \tag{13}$$

is an approximation to the original function. The functions ϕ_k represent the chosen basis, which span a certain functional space, for instance the space of polynomials of degree at most N. The coefficients b_k can be obtained by Galerkin projection or collocation. It is well known that any of these approximations will exhibit true exponential convergence only if f is infinitely differentiable.[9] For the case that f is only piecewise continuous, convergence in maximum norm fails completely, which is one manifestation of Gibbs' phenomenon.

In a series of papers Gottlieb and coworkers have established the possibility of recovering high-order accuracy in maximum norm as $N \to \infty$, i.e. the removal of Gibbs' phenomenon associated with the spectral representation of piecewise smooth functions, see[10,11] and references therein. Results were obtained for both Galerkin and Collocation types, such as the Fourier series and expansion in Chebyshev polynomials. In fact, given the first N exact spectral coefficients exponential convergence in maximum norm as $N \to \infty$ has been proved for any subdomain $[x_1, x_2]$ where the function is analytic, i.e.

$$\max_{x\in[x_1,x_2]} |f(x) - f_N(x)| < e^{-\alpha N} , \qquad \alpha > 0 , \tag{14}$$

so that by juxtaposing the domains of analyticity exponential convergence can be recovered in the complete interval. Formally the method can be summarized as follows. Suppose a projection $P_N(f)$ of the form of equation 13 is given. For piecewise continuous functions, the maximum error of the projection will be of order unity. Suppose now we re-project P_N into another space, spanned by basis functions which we shall denote by Ψ_m^λ (we anticipate here that our new basis functions will be two-parameter families). We seek conditions under which the new projection, which we denote by G_M leads to an exponentially small error in maximum norm, $||.||_\infty$. Consider

$$||G_M P_N f - f||_\infty \leq ||G_M P_N f - G_M f||_\infty + ||G_M f - f||_\infty \tag{15}$$

The second term on the right-hand side measures how well the new basis is suited to approximate the original function f (For the known Gibbs complementary bases one actually needs to show that this approximation converges while *both* parameters of Ψ_m^λ are increased simultaneously). The key step is proving that the first component of the error in equation 15 on the preceding page vanishes exponentially fast. Write this term as

$$||G_M P_N f - G_M f||_\infty = ||G_M (P_N - I) f||_\infty \ . \tag{16}$$

In a sense we thus have a measure of the orthogonality of the new space and the part of the spectrum of the original projection which is not resolved. If these spaces are nearly orthogonal, or become orthogonal at an exponential rate as N is increased, meaning that the unknown high modes have very little effect on the representation in the new projection, the error will decrease exponentially as $N \to \infty$.

In our case, the spectral data is an approximation, obtained by a highly accurate numerical method. This will affect the reconstruction in various ways. For instance stabilizing diffusion or filtering has to be added to the spectral or pseudo-spectral method used to compute the solution, so that instead of equation 16 one has

$$||G_M D^p P_N f - G_M f||_\infty = ||G_M (D^p P_N - I) f||_\infty \ , \tag{17}$$

where we have formally introduced a dissipation or filtering operator of order p, which will operate primarily on the high frequency part of the original projection P_N. The effect of such operators on the reconstruction is still an open problem. Furthermore, details of the numerical implementation, such as, boundary conditions, can be expected to have a profound effect, not considered in the previous theoretical work related to the Gegenbauer reconstruction.

In this work order of accuracy is most often measured by refining the mesh (h-refinement), while keeping the spectral modes (i.e. the number of collocation points) constant in each control volume, whereas most of the previous work has been on spectral convergence, i.e. increasing the total number of spectral modes (p-refinement). This latter point is not expected to be critical, since after all, the fixed-rate convergence of h-refinement is a relaxation of the convergence requirement.

B. A Gibbs-Complementary Basis: The Gegenbauer Polynomials

The first basis which has been identified as Gibbs complementary to, in fact, a whole host of spectral projections, are the Gegenbauer polynomials, $\Psi_m^\lambda = C_m^\lambda$, which are a subset of the Jacobi polynomials, m is the degree of the polynomial, and λ is a second parameter. The Gegenbauer polynomials can be defined as the polynomials, which are orthogonal on the interval $[-1, 1]$ with the weight function $w(x) = (1 - x^2)^{\lambda - \frac{1}{2}}$, i.e.

$$\int_{-1}^{1} C_n^\lambda(x) C_m^\lambda(x) (1 - x^2)^{\lambda - \frac{1}{2}} \, dx = \delta_{nm} h_n^\lambda \ . \tag{18}$$

In the most common form the Gegenbauer polynomials are not normalized,[12] and the constant h_n^λ is given by

$$h_n^\lambda = 2^{1-2\lambda} \pi \frac{\Gamma(n + 2\lambda)}{(n + \lambda)\Gamma^2(\lambda)\Gamma(n + 1)} \ , \tag{19}$$

where $\Gamma(x)$ is the Gamma function.

We will refer to the re-projection of a spectral representation onto Gegenbauer space as the Gegenbauer reconstruction procedure. The Gegenbauer reconstruction operates on each subinterval on which the solution is smooth. Assume for the sake of simplicity that $[-1, 1]$ is such an interval (general intervals can be handled by appropriate scaling). It can be shown that the *truncated* expansion up to order $M < \infty$, based of the *approximation* to f , i.e. the projection $G_M P_N f$

$$f_M = \sum_{n=0}^{M} \widetilde{g}_m^\lambda C_m^\lambda(x) \ , \tag{20}$$

where

$$\widetilde{g}_m^\lambda = \frac{1}{h_m^\lambda} \int_{-1}^{1} (1-x^2)^{\lambda-\frac{1}{2}} f_N(x) C_n^\lambda(x)\, dx \ , \tag{21}$$

and f_N is the original projection of the general form of equation 15 on page 5, converges exponentially fast to f in maximum norm, even at discontinuities, provided the two parameters, M and λ vary linearly with N,

$$M \propto \lambda \propto N \ , \tag{22}$$

where the constants of proportionality depend on the spectral representation of f_N. While the details of the proof are different for different spectral representations, one can roughly argue that the necessity of varying the parameters in this way stems from the trade-off between the obvious fact that the the order of the polynomials has to be increased along with the original projection to achieve spectral convergence, and the need to maintain a reasonable degree of separation between the complement of the original projection and the Gegenbauer space to keep the orthogonality error, equation 16, small.

C. Remarks on the Gegenbauer Basis

Despite the fact that exponential convergence can be proven there are a few well-known problems associated with the Gegenbauer basis, which can have a profound effect in numerical implementations. We will briefly summarize a few points.

- The success of the reconstruction depends on the smoothness of the unknown function. More precisely, the constants of proportionality in equation 22 depend on how far the function can be extended onto the complex plane. In the absence of such information these constants have to be estimated, and for fixed values the reconstruction might fail for certain functions.

- The Gegenbauer polynomials assume very large numerical values very quickly as the parameters are increased. If one wishes, for example, to resolve several periods of a low-frequency oscillation, this can lead to large errors for intermediate orders of approximation. If a fair number of polynomials are included, but not enough to resolve all periods of the oscillation, the approximation will fail (just as it would for any polynomial approximation). But because of the large amplitude of the polynomials the failure can be catastrophic until enough modes are added to resolve the function properly. Only then will the error vanish exponentially fast.

- In numerical implementations the large magnitude of the Gegenbauer polynomials also amplifies the effect of round-off errors. While the numerical values of the polynomials increase dramatically as N is increased, the sum in equation 20, is usually of order unity, so that for large N some coefficients in the truncated sum may need to be smaller than machine accuracy, but at the same time highly accurate to represent the solution with small absolute errors. The shear magnitude of the Gegenbauer polynomials again leads to catastrophic failure for this case.

- The very nature of the Gegenbauer projection leads to difficulties, since it becomes more and more extrapolatory as λ is increased (the weight function approaches a delta function). In the limit of $\lambda \to \infty$ the Gegenbauer series approaches a power series, and only the function value at the midpoint of the domain contributes to the expansion.

D. An Alternative Basis: The Freud Polynomials

Recently, the concept of robust Gibbs complements has been proposed by Tanner and Gelb.[13] The additional requirement is that the associated weight of the new basis converge to a limit which still has an associated set of polynomials that can serve as a basis for an exponentially convergent projection (this is not the case for the Gegenbauer polynomials, since the weight converges to a delta function). The Freud polynomials,

which are orthonormal on the real line with respect to the weight $w(x) = \exp(-cx^{2n})$, have been proposed as an alternative to the Gegenbauer basis, and indeed in preliminary numerical experiments have proven more benign. Unfortunately very little is known about the Freud polynomials, in particular the three-term recurrence relation is not known analytically, which has prevented a rigorous proof that the Freud polynomials can serve as an alternative Gibbs complementary basis. Some elements and numerical evidence, however, have been shown.[13] We will use the Freud polynomials as an alternative to the Gegenbauer polynomials for certain test problems in this work.

E. Multidimensional Extension and Edge Detection

The Gibbs-complementary reconstruction in higher dimensions is very similar to the 1D method, using a tensor product form. However, since it operates on smooth subdomains, more sophisticated domain decomposition techniques and coordinate transformations will have to be used, which poses additional algorithmic challenges. A mapping to at least quadrilateral subdomains is required, which can then be easily mapped to a square to use the tensor product basis based on Gegenbauer or Freud polynomials.

We have omitted so far the issue of identifying discontinuities. Edge detection techniques have been proposed,[14,15] and have been used as part of this work. At least in one dimension these techniques are straight-forward and work very reliably. In essence, the edge detection mechanism used in this work is based on the generalized Fourier conjugate sum

$$S_N^\sigma = \sum_{k=0}^{N} \sigma\left(\frac{k}{N}\right) \left(a_k \sin kx - b_k \cos kx\right) \ , \tag{23}$$

where $\sigma = 1$ corresponds to the classical conjugate sum, and the coefficients a_k and b_k are related to the complex Fourier coefficients f_k via $f_k = a_k + ib_k$. It is known that the classical Fourier conjugate sum converges to

$$-\pi/\log(N) S_N \rightarrow [f(x)] \ , \tag{24}$$

where $[f(x)] = f(x^+) - f(x^-)$. Thus it can be conveniently used to detect discontinuities, where $[f(x)] \neq 0$. The factors $\sigma(x)$ are introduced to accelerate the convergence. Quasi one-dimensional versions of these techniques for higher dimensions have also been proposed. However, the best edge detection algorithm in higher dimensions is still subject to further research.

IV. Numerical Results

A. The Spectral Difference Method for Smooth Solutions

Figure 3 shows a validation of the 2D scheme on the linear advection equation

$$\partial_t u + \partial_x u + \partial_y u = 0 \ , \qquad (x, y) \in [0, 1] \times [0, 1] \tag{25}$$

$$u(x, u, t = 0) = \sin(2\pi(x + y)) \ , \tag{26}$$

with periodic boundary conditions for 2^{nd}, 3^{rd} and 4^{th} order accuracy. The solutions have been computed on triangular meshes, generated from structured N by N meshes by simple triangulation. The nominal accuracy is clearly achieved for all solutions. Simple scalar diffusion for the normal fluxes has been used, while the tangential fluxes have not been averaged, but taken directly from their respective elements. Interior flux points are evaluated directly with the reconstructed solution variables.

For validation for the Euler equations consider first the quasi-one-dimensional flow through a nozzle. The governing equations are given by

$$\frac{\partial w}{\partial t} + \frac{\partial F}{\partial x} + Q = 0 \ , \tag{27}$$

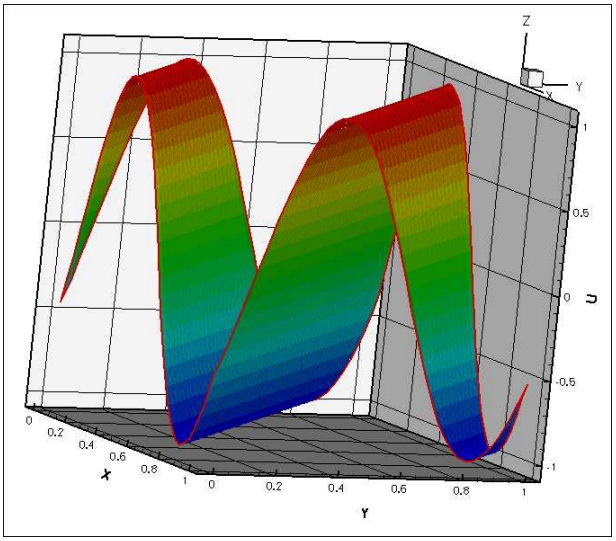

(a) Solution using the Spectral Difference Method on a $30 \times 30 \times 2$ unstructured grid

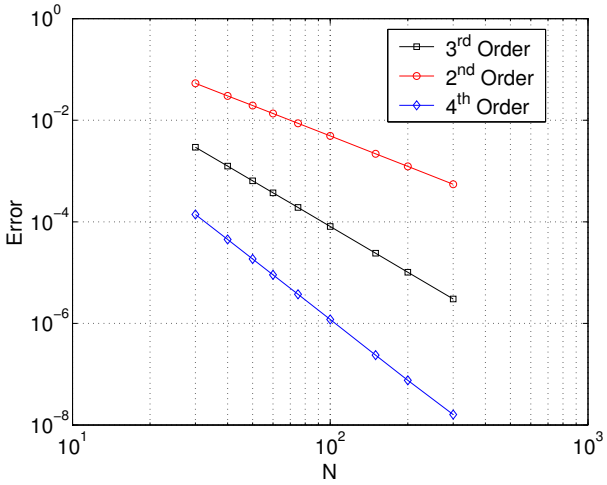

(b) Maximum error in mesh refinement. N is the number of structured mesh points in each direction. There are $N \times N \times 2$ triangles .

Figure 3. Validation of the 2D Spectral Difference Method.

where

$$w = \begin{pmatrix} \rho \\ \rho\, u \\ E \end{pmatrix} \quad , \quad F = \begin{pmatrix} \rho\, u \\ \rho\, u^2 + p \\ u(E+p) \end{pmatrix} \quad , \quad Q = \frac{1}{A}\frac{\partial A}{\partial x} \begin{pmatrix} \rho\, u \\ \rho\, u^2 \\ u(E+p) \end{pmatrix} \quad , \tag{28}$$

where A is the cross-section of the domain. Figure 4 on the following page shows the steady-state entropy error in h-refinement and p-refinement for isentropic nozzle flow as computed by the spectral difference method. The flow conditions have been chosen such that the nozzle exit Mach number is $M = 0.3$, and the nozzle geometry such that the flow is subsonic everywhere. The maximum Mach number in the throat is $M \approx 0.46$. It can be seen that for the the 3^{rd} order method shown in figure 4(a) the error decreases at the nominal rate in mesh refinement. For this test case no limiters have been used, and the dissipation coming from the element boundaries is sufficient to stabilize the solution. The CUSP construction of artificial dissipation has been used. For interior flux points the flux function is directly evaluated with the reconstructed solution variables, hence single valued.

To test the Spectral Difference Method for the 2D Euler equations, consider subsonic flow around the NACA0012 airfoil. Figure 5 shows results for a 3^{rd} order Spectral Difference scheme at flow conditions $M = 0.3$ and zero angle of attack. In figure 5(a) we show Mach number contours. We point out that the contour plot does *not* use the spectral information in the solution, but merely uses a simple scattering to the original nodes of the mesh to visualize the data. Figure 5(b) shows the distribution of entropy along the airfoil for a mesh with 2560 and 10240 triangles. For the third order scheme this corresponds to 15360 and 61440 degrees of freedom (DOF), respectively, since there are six solution nodes to each triangle. Figure 5(c) compares this data with results from a finite volume scheme, which employs the CUSP scheme with a SLIP data reconstruction,[5] and uses the triangles as control volumes. Note that these are merely isolated results and do not represent an attempt to carry out a mesh refinement study. The mesh has *not* been isotropically refined, but merely "best-practice" meshes have been used. Note that the entropy error for the spectral difference scheme with 15,360 DOF is roughly equal to the entropy error of the finite-volume scheme with

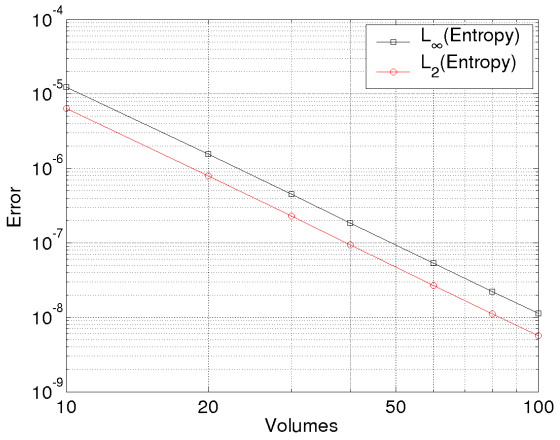

(a) Quasi-1D nozzle flow: Entropy error in h-refinement for the 3^{rd} order Spectral Difference method

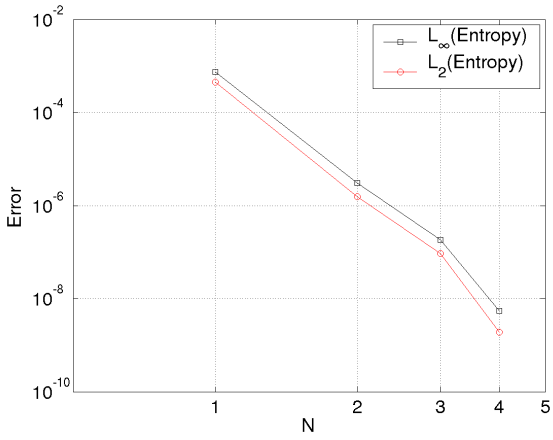

(b) Entropy error in p-refinement for quasi-1D nozzle flow on a mesh with 40 elements.

Figure 4. Validation of the Spectral Difference Method: Quasi-1D nozzle flow.

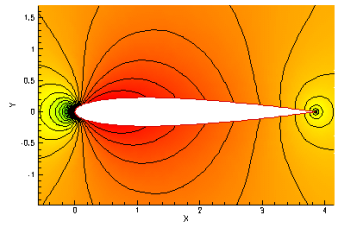

(a) Mach number contours.

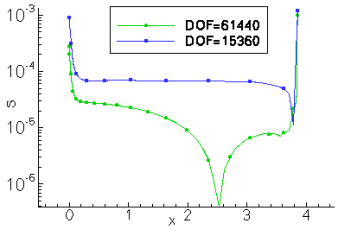

(b) Entropy error along the airfoil For 3^{rd}-order Spectral Difference Scheme with .

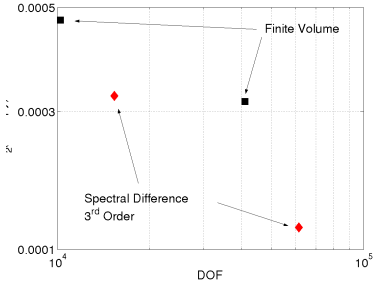

(c) RMS value of entropy along airfoil for several solutions of finite-volume and Spectral Difference schemes. The data is plotted against total degrees of freedom.

Figure 5. Validation of the Spectral Difference Method: Subsonic flow around the NACA0012 airfoil.

approximately 40,000 DOF. No limiters have been used for this testcase.

B. Results for Discontinuous Solutions

As a convenient model equation first consider Burgers' equation with periodic boundary conditions

$$u_t + uu_x = 0 \tag{29}$$

$$u(x,0) = 1 + \tfrac{1}{2}\sin(\pi x)\ , \qquad -1 \le x \le 1\ . \tag{30}$$

Even though the initial conditions are smooth, the solution will develop a discontinuity at finite time. Results for a fifth order accurate Spectral Difference method at $t = 1$, at which time the solution is discontinuous, are shown in figure 6 and figure 8 on page 13. Figure 6(a) shows the solution using $N = 200$ spectral

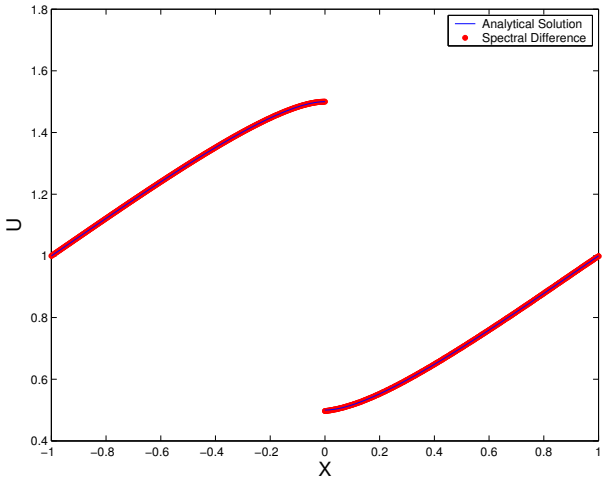

(a) Solution using the Spectral Difference Method with 200 Spectral Elements and the Gegenbauer procedure

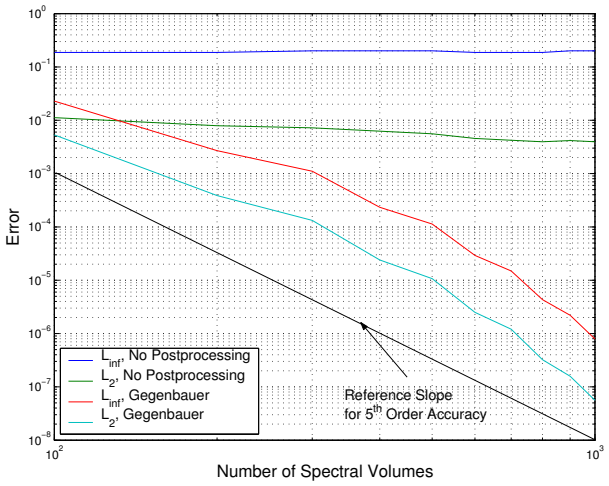

(b) Error with and without Gegenbauer postprocessing

Figure 6. Globally high-order accurate solutions for Burgers' Equation using the Spectral Difference Method and the Gegenbauer Procedure

volumes after reprojection of the solution onto Gegenbauer polynomials. The effectiveness of the procedure is demonstrated by figure 7, where a comparison of the original numerical solution with the expansion in Gegenbauer polynomials is shown. A grid refinement study to verify the nominal order of accuracy as N is increased has been carried out, and is shown in figure 6(b) together with a reference slope indicating the required reduction in global error measures for the nominal fifth order of accuracy. It can be seen that while the original solution fails to converge in maximum norm, and the L_2 norm of the Error barely reaches first order, the re-projected solution converges in both L_2 and maximum norm. It should be emphasized that error norms were computed using *all* nodes in the mesh, so that all global error measures include the discontinuity. The slope of the errors, however, is not constant, which can be explained by the fact that the parameters of the Gegenbauer polynomials, i.e. the order and second parameter λ, have to be adjusted as the mesh is refined. In theory one ought to make the number of Gegenbauer modes proportional to the number of original spectral modes. These, however, remain constant here, because the order of approximation is fixed, i.e. we are carrying out h-refinement instead of p-refinement. It seems most fitting to make the parameters proportional to the total number of collocation nodes. The dependence of the parameters as a function of the number of spectral volumes is depicted in figure 8(b) on page 13. It should be pointed out at this point that

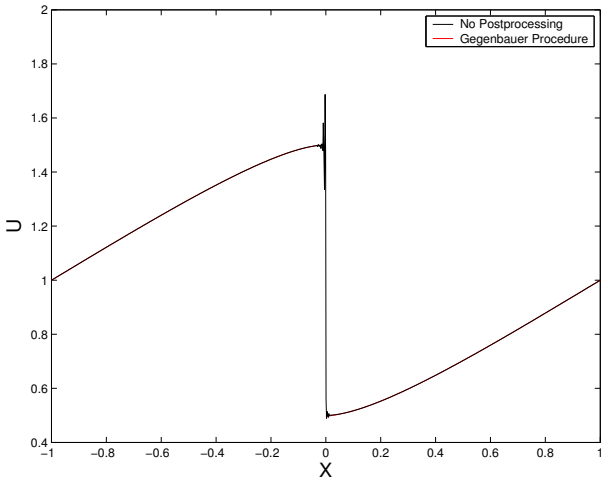

(a) Solution using the Spectral Difference Method with 200 Spectral Elements with and without Gegenbauer postprocessing

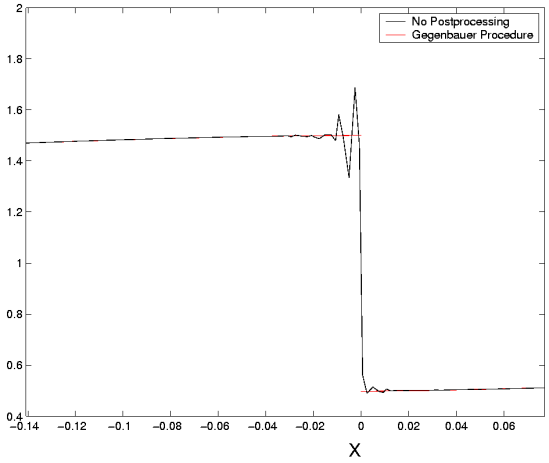

(b) Close-up view of the solution near the discontinuity with and without the Gegenbauer procedure

Figure 7. Globally high-order accurate solutions for Burgers' Equation using the Spectral Difference Method and the Gegenbauer Procedure

the parameters are not optimized in any way, but merely represent "best practice" values. Some suggestions regarding their optimization have been made in the literature.[17]

Figure 8(a) on the following page shows the pointwise errors for the smooth subdomain $-1 \leq x \leq 0$. It can be seen that the error decreases according to the nominal order of accuracy up to the endpoints of the domain, the right endpoint being the discontinuity at $x = 0$.

A further reduction of the maximum error, i.e. below roughly $1. \cdot 10^{-8}$ could not be achieved, due to the inherent numerical problems mentioned in section III. In fact, if the mesh is further refined the error increases and diverges in the limit $N \to \infty$ if the Gegenbauer parameters are further increased, although this can be prevented if the parameters are frozen. For the case of 1000 spectral volumes the order of the polynomials is $m = 25$ and $\lambda = 10$. The value of the corresponding Gegenbauer polynomial at $x = 1$ is $C_{25}^{10}(1) = 1.4 \cdot 10^{+12}$. Further refinement increases these numbers, and it becomes clear how it is increasingly difficult to achieve an absolute precision of at least twenty orders of magnitude below the computed values of the Gegenbauer polynomials.

No limiters have been used for these computations, which means that we have relied solely on the dissipation from the fluxes at element boundaries to stabilize the solution. This approach, while acceptable for low-order of accuracy must necessarily fail for p-refinement, i.e. as the degree of spectral approximation is increased. We show below that alternatively a spectral adaptive filtering procedure can be used to stabilize the solution.

As an alternative to Gegenbauer polynomials the Freud polynomials can be used to perform Gibbs-complementary reconstruction. We have carried out two tests for the Burgers' equation. Firstly we solve the equations by a Fourier spectral method using a straight spectral differentiation along with an exponential filter to stabilize the solution. Secondly we use the 5^{th} order Spectral Difference method. These two approaches allow us to test the Freud reconstruction procedure in p-refinement and h-refinement. The results of the refinement studies are shown in figure 9 on the next page. While the maximum errors can be reduced to about the same level as for the Gegenbauer reconstruction method, the numerical behavior is generally more benign for the Freud reconstruction.

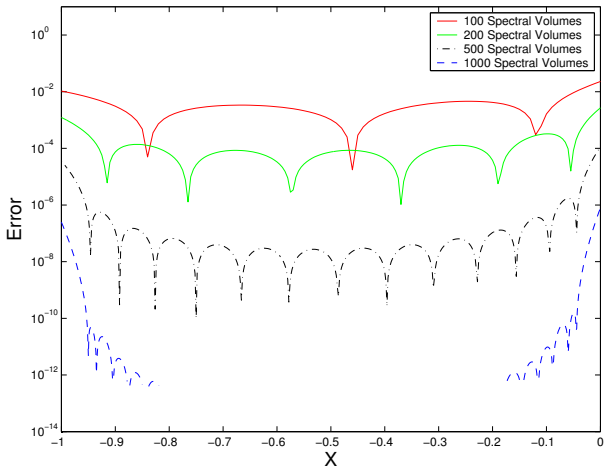

(a) Pointwise Error for several numbers of Spectral Volumes

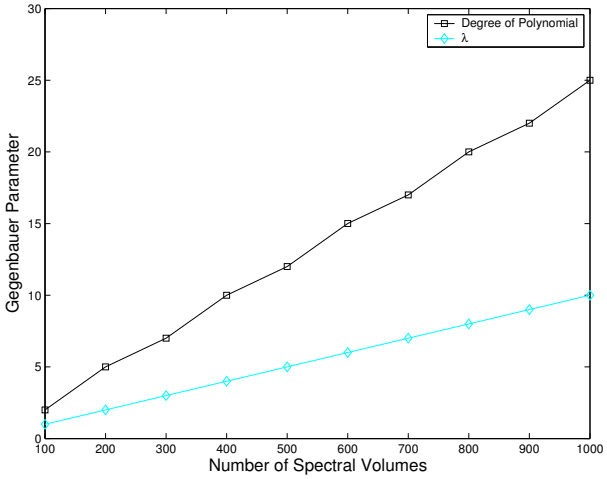

(b) The Gegenbauer Order and second parameter λ as the mesh is refined

Figure 8. Globally high-order accurate solutions for Burgers' Equation using the Spectral Difference Method and the Gegenbauer Procedure

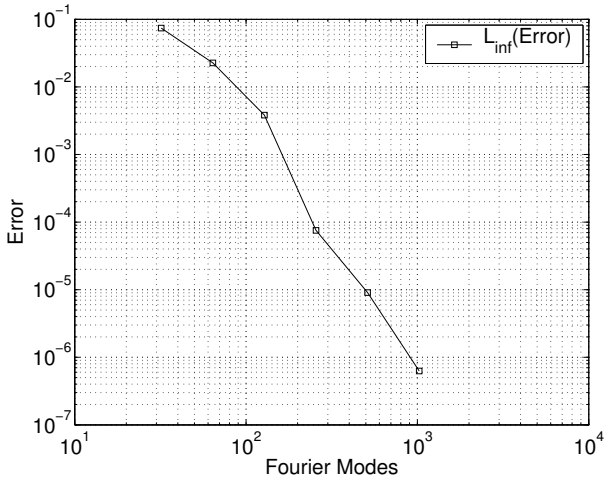

(a) Maximum error in p-refinement for Fourier Spectral Method for Burgers' equation

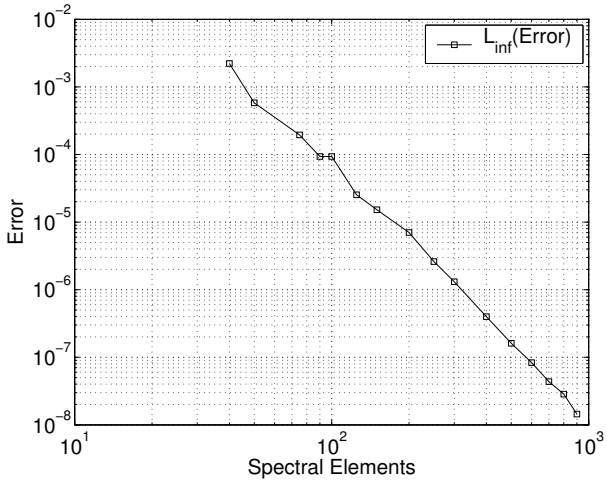

(b) Maximum error in h-refinement for 5^{th}-order Spectral Difference Method.

Figure 9. The Freud reconstruction method for Burgers' Equation

As a preliminary testcase for the Euler equations the Sod shocktube problem has been considered. Figure 10 shows the solution obtained with a fourth-order spectral difference method with scalar diffusion at

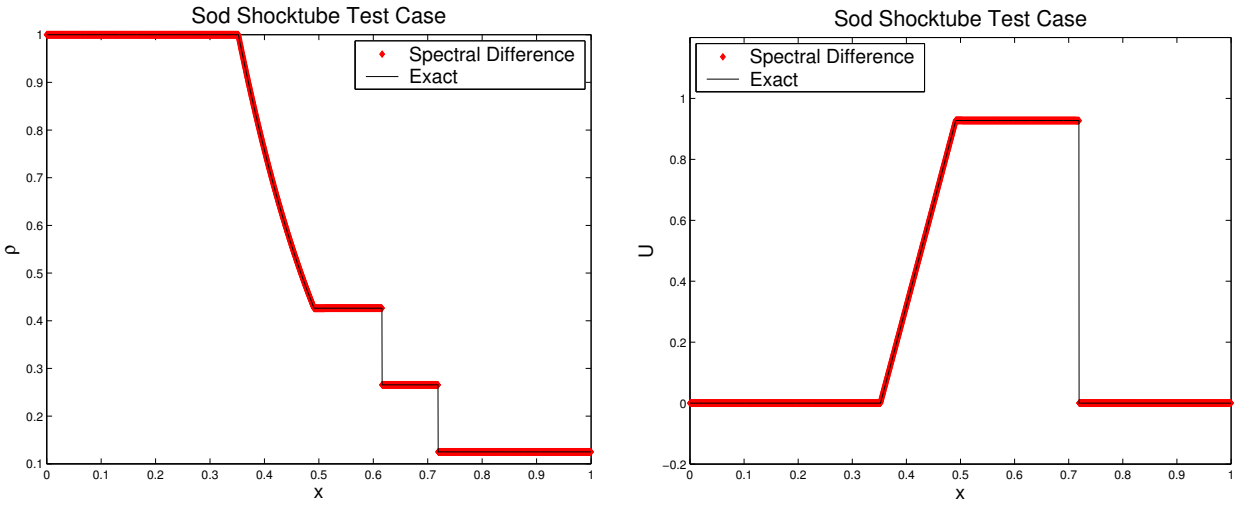

(a) Density

(b) Velocity

Figure 10. Solution for the Sod shocktube case using 800 Elements

element boundaries, along with Butcher-Runge-Kutta time integration. It can be seen from the figure that the shocks and the contact discontinuity are perfectly captured. No limiter or spectral diffusion has been used, which means that the dissipation from the element boundaries must suffice to stabilize the solution. This might be the reason that the maximum error, e.g. in density, could not be reduced beyond approximately $L_\infty(\rho - \rho_{exact}) \approx 1 \cdot 10^{-3}$. However, note that this level of error represents the maximum error in the domain, including the discontinuities. The best way to stabilize the scheme will be the subject of further research. To demonstrate the effect of the reconstruction we show the unprocessed solution along with the reprojected one in figure 11 on the next page. The unlimited original solution, computed by the 4^{th} order spectral difference method, exhibits oscillations of the order of what one would expect from Gibb's phenomenon, if the analytical solution were to be expanded in smooth basis functions.

Naturally, the Spectral Difference method can also be used with conventional limiting functions. While this reduces the accuracy near discontinuities such concepts are comparatively well established and understood. Figure 12(a) shows the solution for quasi-1D nozzle flow with a shock in terms of the density, computed with a 4^{th} order Spectral Difference method and a minmod limiter. Good shock capturing capabilities can be observed. Figure 12(b) shows the Entropy error for the 3^{rd} order and 4^{th} order schemes. While the entropy behind the shock is constant, fixed by the shock jump conditions, the entropy in front of the shock should decrease with increasing accuracy. Indeed it does so, with slight spikes visible at the nozzle throat. This is due to the fact that a TVD (total variation diminishing) limiter has been used, which is active at smooth extrema. This could be removed by using a total variation bounded version of the limiter (TVB). This is planned for future work.

V. Conclusion and Future Work

First steps toward high-order accurate solutions for conservation laws with discontinuous solutions have been shown. The extension to higher dimensions will be a focus of research. So far only the spectral difference

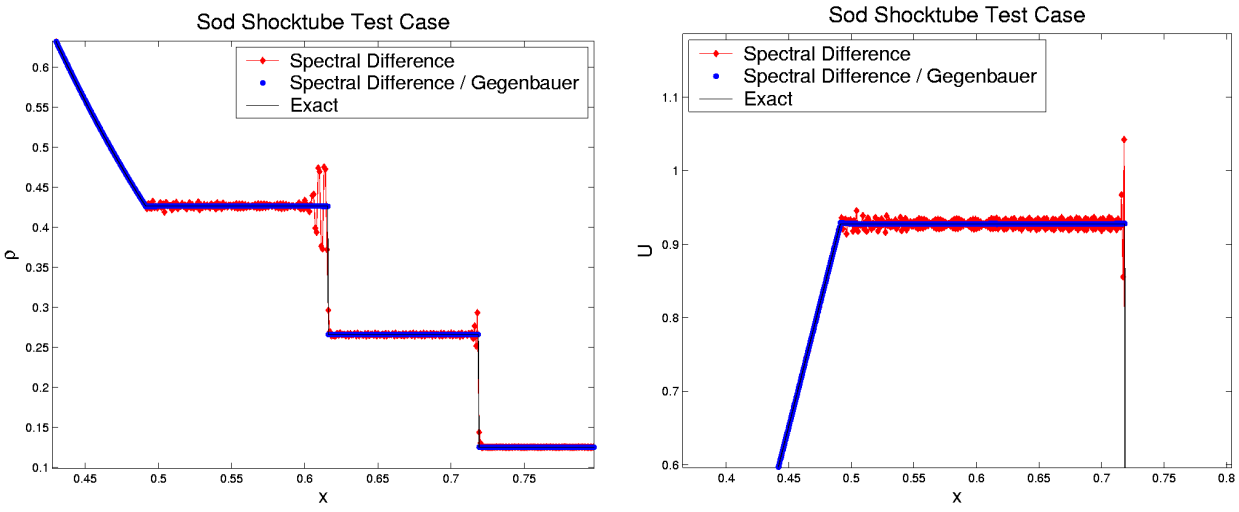

(a) Density

(b) Velocity

Figure 11. Solution for the Sod shocktube case using 800 Elements.

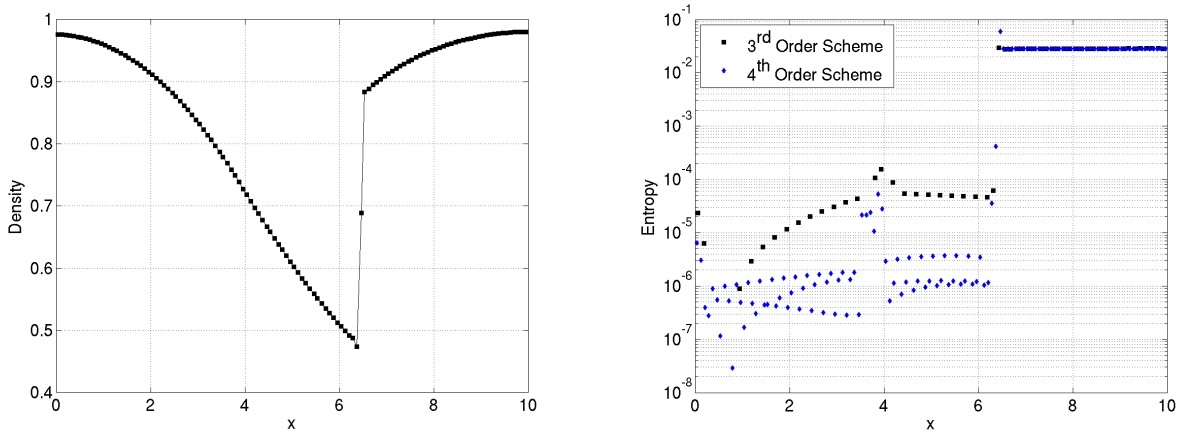

(a) Density distribution for the 4^{th} order Spectral Difference Scheme and 40 elements.

(b) Entropy Error for the 3^{rd} and 4^{th} order scheme with 40 elements.

Figure 12. Solution for nozzle flow with a shock using the Spectral Difference method with a minmod limiter.

method has been used, but we will also consider spectral methods. The nature of the Gibbs-complementary reconstruction seems to be well suited for use with spectral and multidomain spectral methods. The extension to viscous fluid flow is another important issue that will be considered in the future.

VI. Acknowledgements

This work has been supported in part by Stanford University through a Stanford Graduate Fellowship (SGF).

References

[1]Liu, Y., Vinokur, M., and Wang, Z. J., "Discontinuous spectral difference method for conservation laws on unstructured grids," *Proceedings of the 3rd International Conference on Computational Fluid Dynamics, July 12-16, 2004, Toronto, Canada*, Springer, 2004.

[2]Wang, Z. J. and Liu., Y., "The Spectral Difference Method for the 2D Euler Equations on Unstructured Grids," Aiaa paper 2005-5112, 2005.

[3]Kopriva, D. A., "A Conservative Staggered-Gri Chebyshev Multidomain Method for Compressible Flows II: Semi-Structured Method," *J. Comp. Phys.*., Vol. 128, 1996, pp. 475.

[4]Hesthaven, J. S., "From Electrostatics to Almost Optimal Nodal Sets for Polynomial Interpolation in a Simplex," *SIAM J. Num. Anal.*, Vol. 35, No. 2, 1998, pp. 655–676.

[5]Jameson, A., "Analysis and design of numerical schemes for gas dynamcics 2: Artificial diffusion and discrete shock structure," *Int. J. Comp. Fluid. Dyn.*, Vol. 5, 1995, pp. 1–38.

[6]Cockburn, B. and Shu, C. W., "TVB Runge-Kutta Local Projection Discontinuous Galerkin Finite Element Method for Consrvation Laws II: General Framework," *Math. Comp.*, Vol. 52, No. 186, 1988, pp. 411–435.

[7]Tadmor, E., "Convergence of Spectral Methods for Nonlinear Consrvation Laws," *SIAM J. Num. Anal.*, Vol. 26, No. 1, 1989, pp. 30–44.

[8]Gottlieb, D. and Hesthaven, J. S., "Spectral Methods for Hyperbolic Problems," *J. Comp. Appl. Math*, Vol. 128, 2001, pp. 83–131.

[9]Gottlieb, D. and Orszag, S. A., *Numerical Analysis of Spectral Methods: Theory and Applications*, CBMS-NSF Regional Conference Series in Applied Mathematics, 1977.

[10]Gottlieb, D. and Shu, C. W., "On the Gibbs Phenomenon V: Recovering exponential accuracy from collcoation point values of a piecwise analytic function," *Numer. Math.*, Vol. 71, 1995, pp. 511–526.

[11]Gottlieb, D. and Shu, C. W., "On the Gibbs Phenomenon and its Resolution," *SIAM Rev.*, Vol. 39, No. 4, 1997, pp. 644–668.

[12]Bateman, H., *Higher Transcendental Function, Vol 2*, McGraw Hill, 1953.

[13]Tanner, J. and Gelb, A., "Robust reprojection methods for the resolution of Gibbs phenomenon," *Appl. Comput. Harm. Anal. (preprint)*, 2004.

[14]Gelb, A., "Detection of Edges in Spectral Data," *Appl. Comp. Harm. Anal.*, Vol. 7, 1999, pp. 101–135.

[15]Gelb, A. and Tadmor, E., "Detection of Edges in Spectral Data II. Nonlinear Enhancement," *SIAM J. Numer. Anal.*, Vol. 38, No. 4, 2000, pp. 1389–1408.

[16]Bhatnagar, P., Gross, E., and Krook, M., "A model for collision processes in gases I: Small amplitude processes in charged and neutral one-component systems," *Phys. Rev.*, Vol. 94, 1954, pp. 511.

[17]Gelb, A., "Parameter Optimization and Reduction of Round-Off Error for the Gegenbauer Reconstruction Method," *J. Sci. Comp.*, Vol. 20, No. 3, 2004, pp. 433–459.